The Meteoritical Society

Meteoritics & Planetary Science 52, Nr 3, 532–545 (2017)
doi: 10.1111/maps.12812-2531

Recovering 3D particle size distributions from 2D sections

Jeffrey N. CUZZI[1,*] and Daniel M. OLSON[2]

[1]Ames Research Center, NASA, Moffett Field, California 94035, USA
[2]BAERI, inc., Petaluma, California 94952, USA
[*]Corresponding author. E-mail: jeffrey.cuzzi@nasa.gov

(Received 18 February 2016; revision accepted 12 November 2016)

Abstract–We discuss different ways to convert observed, apparent particle size distributions from 2D sections (thin sections, SEM maps on planar surfaces, etc.) into true 3D particle size distributions. We give a simple, flexible, and practical method to do this; show which of these techniques gives the most faithful conversions; and provide (online) short computer codes to calculate both 2D-3D recoveries and simulations of 2D observations by random sectioning. The most important systematic bias of 2D sectioning, from the standpoint of most chondrite studies, is an overestimate of the abundance of the larger particles. We show that fairly good recoveries can be achieved from observed size distributions containing 100–300 individual measurements of apparent particle diameter.

INTRODUCTION

Proper determination of particle size distributions in chondrites—for chondrules, CAIs, and metal grains—is of basic importance for assessing the processes of formation and/or of accretion of these particles into their parent bodies. To date, most information of this sort is gathered from 2D samples cut from a rock such as in microscopic analysis of thin sections, or SEM maps of planar surfaces (Dodd 1976; Hughes 1978a, 1978b; Rubin and Keil 1984; Rubin and Grossman 1987; Grossman et al. 1988; Rubin 1989; Metzler et al. 1992; Kuebler et al. 1999; Nelson and Rubin 2002; Schneider et al. 2003; Hezel et al. 2008; Fisher et al. 2014; for an exhaustive review with numerous references see Friedrich et al. 2014). While qualitative discrimination between chondrite types can readily be done using data of this sort, any deeper exploration of the processes by which chondrite constituents were created or emplaced into their parent requires a more quantitative approach.

BASIC METHODOLOGY

For simplicity we will consider that the particles can be approximated by spheres (discussed further below). There are well-known sampling effects which cause the observed property $N_A(d)$, the number of particles with apparent diameter d per unit area, to differ from the more fundamental, desired quantity $N_V(D)$, the number of spheres of true diameter D per unit volume. Specifically, sections tend to cut particles nondiametrically, diminishing the fraction at true diameter D and artificially increasing the fraction at smaller apparent diameters. It can be shown from geometry alone that, for a monodispersion of spheres having true diameter D_o, random sectioning produces a distribution $N_A(d)$ with modal apparent diameter $d = \pi D_o/4$ (Weibel 1979, ch. 2). However, even in this simple case, the distribution of apparent diameters is more complicated than a mere shift of the sphere distribution. In a second effect, large objects are overrepresented in apparent diameter distributions. Correcting fully for these effects is straightforward, but the literature is somewhat confusing and there are a number of approaches to doing the same thing, with subtly different notation. This note attempts to clarify and codify the approach, with citations to what we have found to be the most helpful books and articles (some recent, some not) on the subject, and give some tips as to the number of apparent diameter observations needed for good results. In the meteoritics literature the most recent and most widely cited study is by Eisenhour (1996); however, the problem is widely discussed in even greater detail in several other fields, especially biology and materials science, where it is but one part of the discipline of "Stereology," or inferring 3D properties of often much

more complicated structures from observed 2D sections. In fact, the earliest treatment is in the study of red blood cells (Wicksell 1925). The clearest and most useful books we have found, which cover most of the recent important developments, are by Weibel (1979, 1980).

The problem can be broken down into several distinct steps. If the particles can be considered spheres, the basic transformations are very simple. One needs to allow for (1) the off-center sectioning effect above, (2) the fact that a given large particle is sampled by random plane sections more frequently than a given small one, and (3) some implications of section thickness. Eisenhour (1996) deals with (1)–(3), although we think the approach described herein has greater flexibility and is easier to use. To a higher degree of complexity, (4) if the particles are randomly oriented ellipsoids, their axial ratios can also be backed out in a similar way (Cruz-Orive 1976, 1978, 1983; Weibel 1980; Liang and Enfield 2011); this situation is different from known cases where parent body plastic compression and distortion has turned an initial set of spheres into a set of ellipsoids sharing a common orientation. We will not discuss either degree of sophistication here, restricting our application to undeformed, equidimensional particles which can be approximated by spheres. In addition, Cruz-Orive (1976, 1978, 1983) also gives expressions for the best estimate of the variance or standard error associated with the derived values of $N_V(D)$. In earlier papers and sources, including Cruz-Orive (1976, 1978), it is usually stated that these inversion techniques are only valid for low particle volume density because they assume Poisson properties. However, in a good review article, Cruz-Orive (1983) cites more recent work to show that low particle density is not a requirement; it is only required that the statistical properties are invariant from one section to another.

In all applications the different properties $N_A(d)$ and $N_V(D)$ are binned the same way, into a set of diameter bins with lower and upper boundaries at (d_{i-1}, d_i), with d_1 representing the top end of the smallest particle size bin.[1] The N bins can be arithmetically or geometrically spaced, or even have a more general distribution (Cruz-Orive 1983). We will assume for most purposes that the binning is regular, so either $d_i = d_{i-1} + \Delta$, with $\Delta = D_{\max}/N$ (arithmetic), or $d_i = d_{i-1}c$, with $c = (D_{\max}/D_{min})^{1/N}$ (geometric). The geometric binning is used in much of the original work (Wicksell 1925; Saltykov 1967), and the arithmetic binning in more recent work (see Underwood 1970; Weibel 1979, 1980, for excellent background). In arithmetic binning, the number of particles per bin is simply proportional to the more fundamental number per unit diameter, whereas in geometric binning, the number per bin must be divided by the (variable) bin width to give the number per unit diameter. However, we will find that one form of geometric binning provides the optimum recovery.

[1]Some treatments, notably Saltykov (1967), reserve index 1 for the *largest particle*; this minor difference leads to a more cumbersome notation and is not adopted by most recent descriptions of the technique.

The Forward Problem

The simplest way to understand the technique is to consider the "forward problem": how a true diameter distribution $N_V(D_j)$ is manifested in a distribution of apparent diameters $N_A(d_i)$ taken from a section or sections. Note that subscript j refers to a bin number for true diameters D, and subscript i to a bin number for apparent diameters d. Both apparent diameters and true diameters share the same bin boundaries (but in some cases the nominal diameter is in the center of a bin). The sampling process can be written as a sum, in which each apparent diameter bin contains weighted contributions from spheres in a range of true diameter bins of the same size or larger:

$$N_A(d_i) = \Sigma_{j=i}^{N} F_{ij} N_V(D_j). \quad (1)$$

Creating a matrix F_{ij} is a convenient mathematical shorthand for representing how each sphere of diameter D is represented in smaller *apparent* diameter bins by the sampling process; note that F_{ij} has dimensions of length. It is the product of a nondimensional probability P_{ij} that a measured apparent diameter d_i has come from a sphere of diameter D_j, and a dimensional sample weighting factor. Consider first the probability term P_{ij}. A set of planes randomly intersects a target sphere of diameter $D_j = j\Delta$ at different distances z from its center along a diameter, with equal probability per unit length $P(z) = 1/D_j$, *given that it intersects the given particle*. The probability of the resulting apparent diameter lying in a bin of width or thickness $dz_{ij} = |z_{i,j} - z_{i-1,j}|$, is $P_{ij}(z_{i,j} - z_{i-1,j}) = 2|z_{i,j} - z_{i-1,j}|/D_j$ (see Fig. 1); the factor of 2 allows for the fact that random planes can cut at the same distance from the center in two places. Because $z_{i,j} = (D_j^2 - d_i^2)^{1/2}/2$ for spherical particles, $P_{ij}(z_{i,j} - z_{i-1,j})$ can be written directly as $P_{ij}(d_i, d_{i-1})$.

Because a given large particle is sampled more often than a given small particle, at a rate proportional to its diameter, $F_{ij} = D_j P_{ij}$ (Underwood 1970, section 4.3.4; Weibel 1979, section 2.6; Weibel 1980, ch. 6); the factor D_j provides the correct dimensional scaling between $N_A(d_i)$ (cm^{-2}) and $N_V(D_j)$ (cm^{-3}). Imagine, for instance, a volume of side $D_{\max}$, containing just one sphere of diameter $D_{\max}$ and one sphere of much smaller diameter $D(j)$; they have the same N_V but for any total number of cuts through the volume, the smaller sphere contributes a

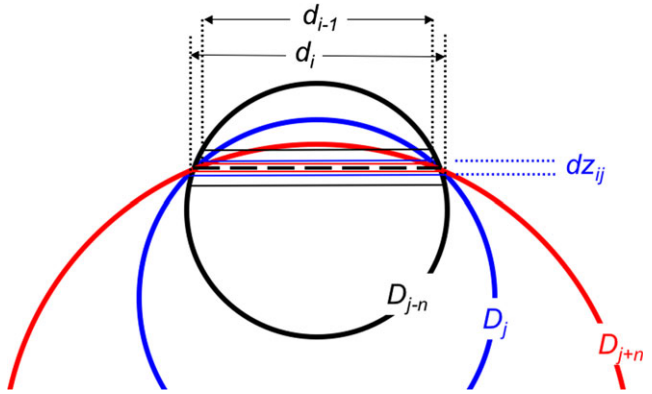

Fig. 1. This sketch shows several ways to get the same chondrule *apparent* diameter, from chondrules of different true diameter. The black dashed line shows one apparent diameter measurement (viewed in its plane) falling in the bin (d_{i-1}, d_i). Three different size chondrules are shown, of true diameter D_{j-n}, D_j, D_{j+n}. Because of their different sizes, the probability $P_{ij} = 2dz_{ij}/D_j$ that each can contribute to an apparent diameter lying within (d_{i-1}, d_i) decreases with increasing diameter. From simple geometry, $z = (D^2 - d^2)^{1/2})/2$ is the distance of the section from the center of the chondrule, and $dz_{ij} = ((D_j^2 - d_{i-1}^2)^{1/2} - (D_j^2 - d_i^2)^{1/2})/2$. Here, the suitable range dz_{ij} is labeled only for the (blue) chondrule with diameter D_j. The probability $P_{i,j-n}$ that the black chondrule of size D_{j-n} can contribute (the normalized distance between the horizontal black lines) is clearly larger, and the probability $P_{i,j+n}$ that the large red chondrule can contribute (the normalized distance between the horizontal red lines) is clearly smaller. These probabilities are the matrix elements described in the text and used in the inversion algorithms. (Color figure can be viewed at wileyonlinelibrary.com.)

fraction $D(j)/D_{\max}$ as many profiles to the observed binning as does the large sphere. Note that Equation 3 of Eisenhour (1996) can easily be rewritten in a similar form, but corrects only for off-diametric slicing; that is, both N_o and N'_o of Eisenhour (1996, Equation 3) connote apparent diameters per unit area (see Underwood 1970, ch. 5, for discussions along this line), and the conversion to volume density of real spheres (factor of $1/D_j$) is incorporated as a separate term later in Eisenhour's development. Eisenhour's approach involves an iterative, hands-on procedure correcting one size bin at a time starting with the largest, similar to that of Saltykov (1967). Such recovery approaches are often called *unfoldings*. Here we will emphasize a simultaneous solution for $N_V(D_j)$ in all size bins by a matrix inversion technique, using the matrix $P_{i,j}$ above, that is perhaps more suited to current analysis tools and accomplishes both of these two most significant corrections at once. We refer to our recovery approach as an *inversion*.

A subtlety arises immediately regarding P_{ij}, which has only been recognized in stereology in retrospect. Here we closely follow Weibel (1979, sections 2.8 and 5.2.9; see Weibel 1980, chapter 6, for even more detailed derivations). One can adopt an experimentalist's viewpoint based on discrete binning (Saltykov 1967), or a mathematician's viewpoint based on differential calculus (Wicksell 1925); the apparently best version represents a blend of these (Goldsmith 1967; Cruz-Orive 1978). This difference appears for both arithmetic and geometric binning.

Arithmetic Binning

In the first case, one writes the probability P_{ij} of obtaining an apparent diameter lying between bin boundaries $d_{i-1} = (i-1)\Delta$ and $d_i = i\Delta$, from a sphere of true diameter $D_j = j\Delta$ (see Fig. 1), as

$$P_{ij}(d_{i-1}, d_i) = \frac{2|z_i - z_{i-1}|}{D_j} = \frac{\sqrt{D_j^2 - d_{i-1}^2} - \sqrt{D_j^2 - d_i^2}}{D_j}. \tag{2}$$

In the second case, one writes the probability of finding the apparent diameter d_i, *centered within* a small bin width $\Delta = |d_{i-1/2} - d_{i+1/2}|$, as

$$P_{ij}(d_i, \Delta) = \frac{2|z_{i+1/2} - z_{i-1/2}|}{D_j} = \frac{\sqrt{D_j^2 - d_{i-1/2}^2} - \sqrt{D_j^2 - d_{i+1/2}^2}}{D_j}. \tag{3}$$

The difference would be negligible in the limit $\Delta \to 0$; however, for the moderately coarse binnings we are faced with in practice, it is significant. Similar expressions can be easily derived for geometrical bin spacings (see below). Writing the full coefficient $F_{ij} = D_j P_{ij}$, and substituting the definitions above, we find for the arithmetic binning with apparent diameters lying between bin boundaries as in Equation 2 (Weibel 1979, 1980; Liang and Enfield 2011):

$$F_{ij}(d_{i-1}, d_i) = \sqrt{D_j^2 - d_{i-1}^2} - \sqrt{D_j^2 - d_i^2} = \Delta(\sqrt{j^2 - (i-1)^2} - \sqrt{j^2 - i^2}), \tag{4}$$

or, using the arithmetic centered binning of Wicksell (1925) for apparent diameters as in Equation 3:

$$F_{ij}(d_i, \Delta) = \sqrt{D_j^2 - d_{i-1/2}^2} - \sqrt{D_j^2 - d_{i+1/2}^2} = \Delta\left(\sqrt{j^2 - (i-1/2)^2} - \sqrt{j^2 - (i+1/2)^2}\right). \tag{5}$$

Moreover, Goldsmith (1967) and Cruz-Orive (1978) independently developed a further refinement which is

somewhat of a blend between the two approaches mentioned above, that retains the apparent diameter bin boundaries (d_{i-1}, d_i) but treats the contributing (larger) actual spheres as lying at the center of *their* bins; that is, $D_j = (j - 1/2)\Delta$, leading to coefficients of yet a slightly different form for $F_{ij}(d_{i-1}, d_i) = \Delta(jP_{ij})$:

$$F_{ij}(d_{i-1}, d_i) = \Delta(\sqrt{(j-1/2)^2 - (i-1)^2} - \sqrt{(j-1/2)^2 - i^2}) \text{ for } j = 1, ..i-1,$$
$$F_{ii}(d_i, d_i) = \Delta\sqrt{i - 3/4} \text{ for } j = i. \quad (6)$$

Note that, for the Goldsmith–Cruz-Orive approach (Equations 6) *and* the Wicksell approach (Equation 5), the bin $i = j$ requires special treatment to avoid square roots of negative numbers. This amounts to treating it as a half-width bin with *upper* diameter boundary at the bin *midpoint* where the contributing sphere diameter D_j has been defined. This logic leads (for the terms where $i = j$) to substitution of $i = j - 1/2$ instead of $i = j$ in *only* the second square root of Equations 5 and 6, causing these terms to vanish, and leading to the expression for F_{ii} given in Equations 6. The reader can verify that the same logic, applied to the centered-binning scheme of Equation 5, leads to $F_{ii} = \Delta\sqrt{i - 1/4}$. Weibel (1979, section 5.2.9, table 5.6; 1980, table 6.6) shows that the final formulation of Equations 6 is significantly superior to, at least, that of Equation 4, which is still often used in stereology (including by Eisenhour 1996), and even misplaces the mode of the recovered distribution.

Geometric Binning

Here, following the Saltykov approach where D_j is chosen at the upper apparent diameter bin boundary $D_j = d_i$, but letting *d increase with i* as is more common so that

$$c = d_i/d_{i-1} > 1, \quad (7)$$

the dimensionless probability coefficients P_{ij} and the full coefficients F_{ij} are as usual related by:

$$P_{ij}(d_{i-1}, d_i) \equiv F_{ij}/D_j = \frac{1}{D_j}\left(\sqrt{D_j^2 - d_{i-1}^2} - \sqrt{D_j^2 - d_i^2}\right) = \sqrt{1 - c^{2(i-j-1)}} - \sqrt{1 - c^{2(i-j)}}, \quad (8)$$

where $j \geq i$. Here, the on-diagonal terms $i = j$ are automatically well behaved as both D_j and d_i are taken at the bin upper boundary, so the second square root vanishes and $P_{ii} = \sqrt{1 - 1/c^2}$. Equation 8 compares closely with Eisenhour's Equation 4 for geometrical binning, where $c^2 = 2$ and, as in his Equation 3, his i is our $j - i + 1$. The coefficients obtained this way also numerically agree with those tabulated by Underwood (1970, table 5.5), following Saltykov (1967), in a case where $c = 10^{-0.1}$ (here the absolute value of P_{ij} must be used, and $c \to 1/c$ in Equation 8, as $c < 1$).

This geometrical case may be generalized along the lines of the Cruz-Orive "blended" method which led to Equations 6 above, assuming each contributing sphere D_j to lie at the *geometric midpoint* of its bin, rather than the upper boundary d_j: $D_j = d_1\sqrt{d_{j-1}d_j/d_1^2} = d_1\sqrt{c^{j-2}c^{j-1}} = d_1c^{j-3/2}$ (where d_1 is the upper boundary of the smallest diameter bin). Then

$$F_{ij}(d_{i-1}, d_i) = D_jP_{ij} = D_j(\sqrt{1 - c^{2(i-j-1/2)}} - \sqrt{1 - c^{2(i-j+1/2)}}) = d_1(\sqrt{c^{2j-3} - c^{2i-4}} - \sqrt{c^{2j-3} - c^{2i-2}}), \text{ and}$$
$$F_{ii}(d_i, d_i) = d_1c^i\sqrt{c^{-3} - c^{-4}} = d_1c^{i-3/2}\sqrt{1-c} \text{ for } j = i. \quad (9)$$

The on-diagonal term F_{ii} in Equations 9 is equivalent to $P_{ii} = F_{ii}/D_i = \sqrt{1 - 1/c}$, slightly different than the expression associated with Equation 8. Surprisingly, however, tests show (see below) that the midpoint technique represented by Equations 9 actually works less well than the nominal case of Equation 8 for geometrical binning, even while previous researchers have found that, for arithmetic binning, the midpoint variation works better (Equations 6 versus Equation 4).

The Inversion Technique

The coefficients F_{ij} are the essence of the inversion process and are seen to be defined entirely by the bins chosen; for arithmetic spacings (Equations 6), the bin thickness Δ factors out, so a set of dimensionless coefficients can be applied to a number of problems where the same *number* of bins is adopted, regardless of bin size. Of course, different sets of coefficients would apply to particles of different shapes; Saltykov (1967) gives examples for cubes. Tables of coefficients appear in various books and articles, each specifying a different number of bins and each with slightly different notation; yet, calculating these tables is straightforward in general, using coefficients described above.

Thus, measured apparent diameters resulting from each particle of true diameter D_j contribute a "tail" extending to smaller (but not larger!) apparent diameter bins d_i. Saltykov (1967) and Underwood (1970, section 5.3.3) give a verbal description of how this process is "unfolded" from a sequential standpoint, making use of the fact that the largest profile can only derive from the

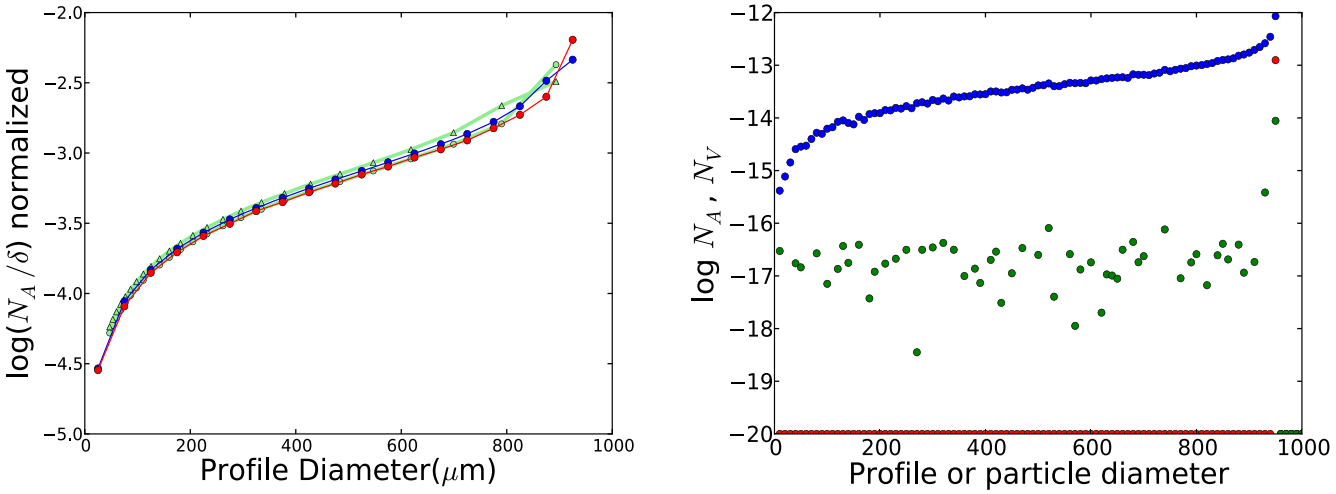

Fig. 2. Left: Histograms of apparent diameter as obtained from an initial δ-function N_{Vo}. Red curve: random numerical sectioning. Blue curve: Equation 1 with the F matrix defined by Equations 6. The red and blue curves are arithmetically binned. Green curve with dots: using Equations 1 and 8 for F; green curve with triangles: using Equations 9. Both green curves are on a geometrically spaced grid. These N_A curves are plotted against the respective arithmetic or geometric midpoints of the bins. When comparing arithmetically and geometrically binned quantities, they must both be converted to an equivalent density per unit diameter, as the bin widths are different. Each curve is normalized by the total number of measurements it contains. Right: inverting the apparent diameter distribution N_A (blue symbols) obtained from a delta function initial N_{Vo} (red symbols, all but one on the lower axis); all distributions are binned into a linear diameter histogram with spacing Δ = 10 μm. The recovered N_V is shown in green symbols. (Color figure can be viewed at wileyonlinelibrary.com.)

largest diameter sphere, and works iteratively from the largest bin through smaller profile size bins by removing contributions from larger (already corrected) true diameter bins. The same approach is advocated in Eisenhour (1996).

However, the process can be expressed more compactly, and automated more cleanly, if expressed as a matrix inversion. If the largest particles are in bin 1, the notation is simpler (Saltykov 1967):

$$\begin{aligned} N_A(d_1) &= F_{1,1}N_V(D_1) \\ N_A(d_2) &= F_{2,1}N_V(D_1) + F_{2,2}N_V(D_2) \\ N_A(d_3) &= F_{3,1}N_V(D_1) + F_{3,2}N_V(D_2) + F_{3,3}N_V(D_3) \\ &\cdots\cdots \end{aligned} \tag{10}$$

where it can be seen that bins of apparent diameter receive contributions only from larger particles. If the largest particles are in bin N and the smallest in bin 1, the notation is:

$$\begin{aligned} N_A(d_N) &= F_{N,N}N_V(D_N) \\ N_A(d_{N-1}) &= F_{N-1,N}N_V(D_N) + F_{N-1,N-1}N_V(D_{N-1}) \\ N_A(d_{N-2}) &= F_{N-2,N}N_V(D_N) + F_{N-2,N-1}N_V(D_{N-2}) \\ &\quad + F_{N-2,N-2}N_V(D_{N-2}) \\ &\cdots\cdots \end{aligned} \tag{11}$$

where in both cases it can be seen that apparent diameter bins receive contributions only from larger particles, and both can be written in the form of Equation 1. Then, extracting the factor Δ from F_{ij} and introducing the notation k_{ij}, we can write for the arithmetic binning

$$\begin{aligned} N_A(d_i) &= \Sigma_{j=1}^{N} F_{ij}N_V(D_j) = \Delta\Sigma_{j=1}^{N}(jP_{ij})N_V(D_j) \\ &= \Delta\Sigma_{j=1}^{N} k_{ij}N_V(D_j), \end{aligned} \tag{12}$$

where now the index can be written as $j = 1,N$ because the terms to one side of the diagonal ($j < i$ in Equation 1) are set to zero. For the geometrical binning we get (introducing the notation g_{ij}):

$$\begin{aligned} N_A(d_i) &= \Sigma_{j=1}^{N} F_{ij}N_V(D_j) = d_1\Sigma_{j=1}^{N}(c^{j-3/2}P_{ij})N_V(D_j) \\ &= d_1\Sigma_{j=1}^{N} g_{ij}N_V(D_j). \end{aligned} \tag{13}$$

Comparing Equations 10 and 11 with 12, we see that $k_{ij} \equiv jP_{ij}$ (in the notation of Weibel 1980) is an upper-triangular matrix in case $d_i = i\Delta$ (smallest particle in bin 1), and a lower-triangular matrix is obtained in the Saltykov (1967) approach where index $j = 1$ denotes the largest particle (Equation 10).[2] Similarly for the geometrical case, $g_{ij} = c^{j-3/2}P_{ij}$ (see Equations 9 and associated discussion). We mention this only as an illustration of different approaches the

[2]Note that a convenient numerical sanity check can be obtained from Equation 12 using $\Sigma_i N_A(d_i) = \Delta\Sigma_j(jN_V(D_j)\Sigma_i P_{ij}) = \Delta\Sigma_j(jN_V(D_j) = \Sigma_j D_j N_V(D_j)$ as $\Sigma_i P_{ij} = 1$.

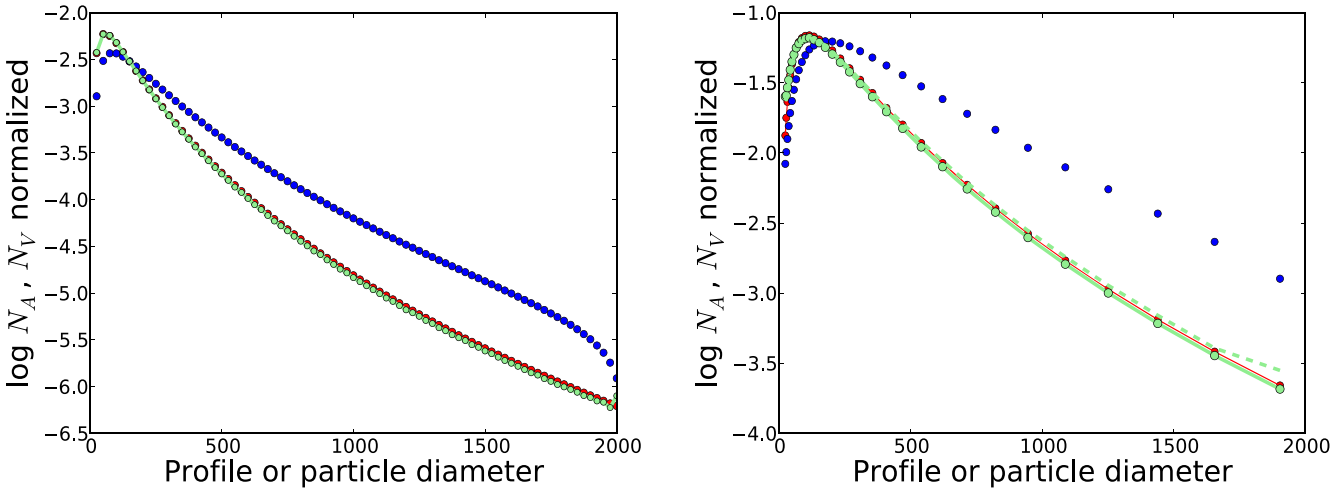

Fig. 3. Results from random sectioning of a lognormal distribution (mean diameter of 160 and width of 160) into an apparent diameter distribution N_A, and then inverting N_A using several different approaches. Left: Arithmetic binning technique of Equations 6; the red curve is the original N_{Vo} distribution, the blue curve is the N_A per bin, and the green curve is recovered from N_A using Equations 6. Note that the number densities are scaled by the total number of counts, respectively. Right: geometrically binned inversions; the initial $N_V(D)$ is red) and the randomly sectioned $N_A(d)$ in blue. The right and left N_V have the same lognormal size distribution, but look different because the bin width grows with diameter in the right-hand plot. The recovered N_V, using the geometric midpoint method (Equations 9) is shown by the green dashed curve and the result obtained using Equation 8 is shown by the green solid curve with symbols. (Color figure can be viewed at wileyonlinelibrary.com.)

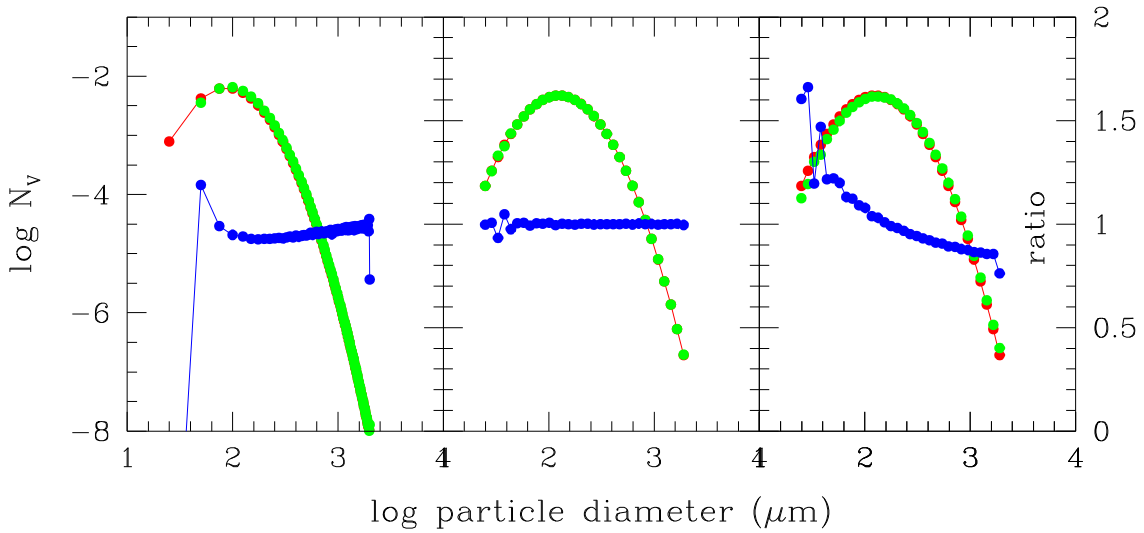

Fig. 4. Sample "observations" of $N_A(d)$ (see Fig. 3) were obtained from 500 k random sections of each bin of an actual lognormal diameter distribution $N_{Vo}(D)$ (red) with mean 150 μm and width 100 μm. The $N_A(d)$ were then inverted into a recovered $N_V(D)$ (green) distribution using (left) the arithmetic method of Equations 6, (middle) the geometric method of Equation 8, and (right) the geometric method of Equations 9. The blue curve plots the ratio N_{Vo}/N_V (right vertical axis); significant slopes in the blue ratio curves (right and left panels) indicate systematic bias of the underlying techniques towards larger or smaller particles. (Color figure can be viewed at wileyonlinelibrary.com.)

reader might encounter; we will deal with upper-triangular matrices and particle diameter increasing with bin number.

The solution for the unknown $N_V(D_j)$ is obtained by inverting the above matrix equation; for the arithmetic binning we get:

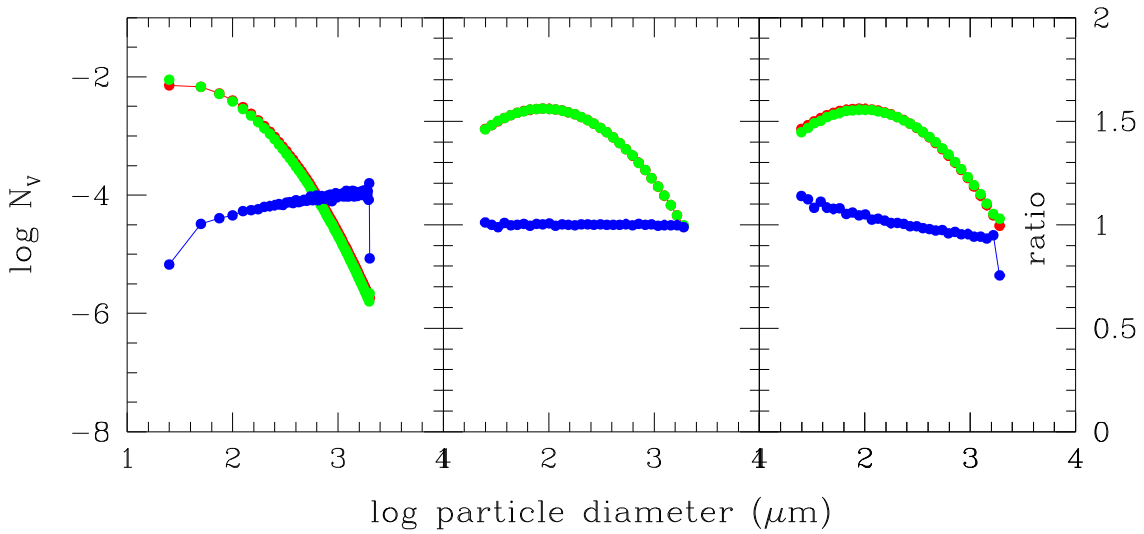

Fig. 5. As in Fig. 4 but for a lognormal N_{Vo} (red) with mean 150 μm and width 200 μm. (Color figure can be viewed at wileyonlinelibrary.com.)

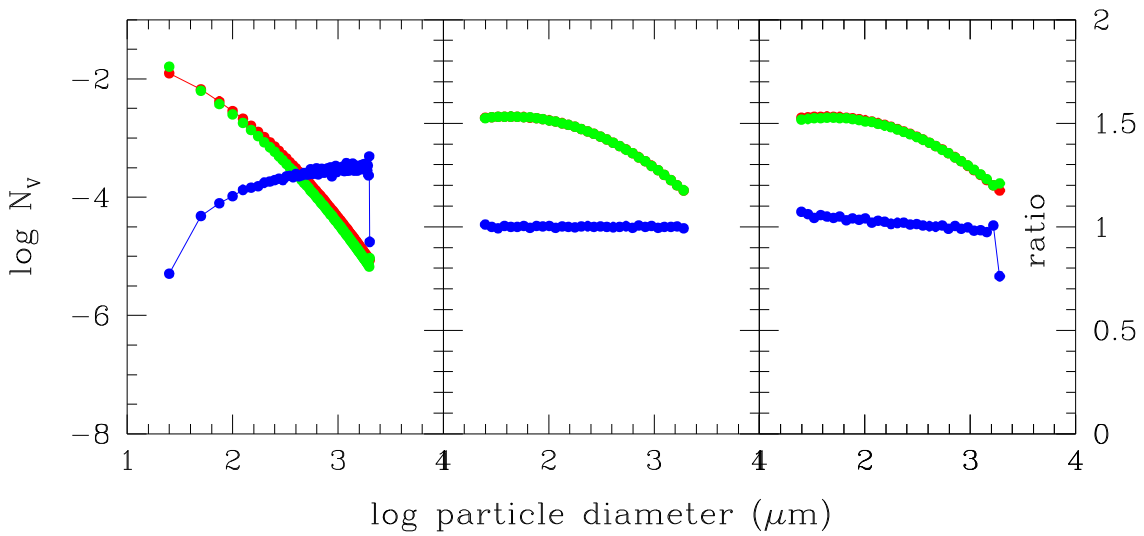

Fig. 6. As in Fig. 4 but for a lognormal N_{Vo} (red) with mean 150 μm and width 500 μm. (Color figure can be viewed at wileyonlinelibrary.com.)

$$N_V(D_j) = \Delta^{-1}\Sigma_{i=1}^{N} k_{ij}^{-1} N_A(d_i), \tag{14}$$

or in the slightly different notation of Cruz-Orive (1976, 1978, 1983)[3] as

$$N_V(D_j) = \Delta^{-1}\Sigma_{i=1}^{N} P^{ji} N_A(d_i), \tag{15}$$

[3]Cruz-Orive uses α as the index representing apparent diameters, and i as the index denoting true diameters.

where P^{ji} is the inverse of P_{ij}; if P_{ij} is upper-diagonal, so is P_{ij}^{-1}. For the geometrical binning $N_V(D_j) = d_1^{-1}\Sigma_{i=1}^{N} g_{ij}^{-1} N_A(d_i)$. Because $F_{ij} = D_j P_{ij}$ is our full correction matrix, and P_{ij} is the analog of Eisenhour (1996) Equation 4, our technique automatically applies Eisenhour's second correction (his Equation 11) for preferential sampling of large particles.

It is tedious but algebraically straightforward to show that the coefficients resulting from the iterative, sequential unfolding given by Saltykov (1967; see also Underwood 1970, section 5.3.3) are exactly the same as the coefficients that result from a matrix inversion (as shown above),

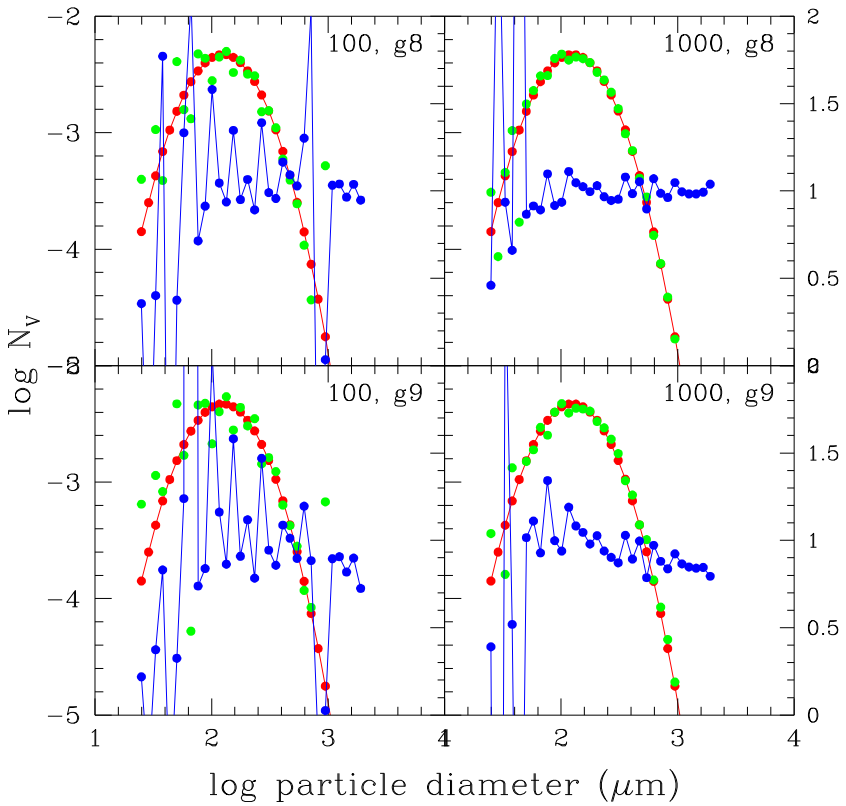

Fig. 7. In this figure each panel has three quantities plotted as a function of upper bin diameter, for a geometrically binned case. The red curve is the initial lognormal distribution $N_{Vo}(D)$ with a mean diameter of 150 μm and width of 100 μm. The green curve is the N_V recovered from a sample N_A computed from random sectioning of the original distribution N_{Vo}. The blue curve is the ratio N_{Vo}/N_V, with scale on the right axis. The number of random cuts used to obtain N_A in each case (N_S, per diameter bin) is labeled on the plots, along with the inversion equation used (g8 or g9). For example, the two upper panels show the N_V recovered using Equation 8, and the N_V in the lower panels used Equations 9. (Color figure can be viewed at wileyonlinelibrary.com.)

starting with the simple, geometrically determined F_{ij} for the binning adopted by Saltykov (in this case F_{ij} and F_{ij}^{-1} are lower-diagonal). We feel it is preferable, given the wide availability of matrix inversion routines in all languages and software packages likely to be used for this analysis, to leave the task of setting up and inverting the matrix, in general, to the reader. However, in the supporting information (Data S1), we provide our own Fortran codes. Tables in Weibel (1979, table 5.6; 1980, table 6.6), or our codes and sample results, can be used to test the numerics of a new code. Weibel (1979, table 5.9) provides $k_{ij} = jP_{ij} = F_{ij}/\Delta$ and his table 5.8 provides the related coefficients $\alpha_{ij} = (jP_{ij})^{-1}$ using the coefficients of Cruz-Orive (1978; for the binning of our Equations 6); these can be adopted and used directly, if 15 arithmetically spaced bins are adequate, as will be true in many cases. It is easily verified that the coefficients k_{ij} in table 5.9 agree with Equations 6; the same tables are reproduced in Weibel (1980, tables 6.7–6.8).

The implications of the finite thickness of 2D sections (such as microscope thin sections) have been dealt with in the stereology literature, and by Eisenhour (1996). The formal treatments in the stereology literature (Goldsmith 1967; Underwood 1970; Weibel 1979, ch. 2; Cruz-Orive 1983) seem exclusively to treat the matrix of the finite thickness section as transparent; that is, the effect of thickness is simply to add more profiles of particles of all sizes, although Weibel (section 5.2.4) mentions a different form and effect. The transparent matrix case is not obviously relevant for meteoritical thin sections, where chondrules are closely packed, sections are generally cut thin enough that overlapping chondrule measurements are not a problem, and where matrix is likely to be opaque. Eisenhour (1996) mentions cases of both transparent and opaque matrix, but in the end his quantitative correction refers only to the (more realistic) opaque matrix case. This would seem to be a good subject for future study. In many cases of interest (SEM or photomicrography for instance), plane front-surface sections are used rather than "slices" of small but finite thickness, avoiding this problem and the need to correct for it. Cruz-Orive

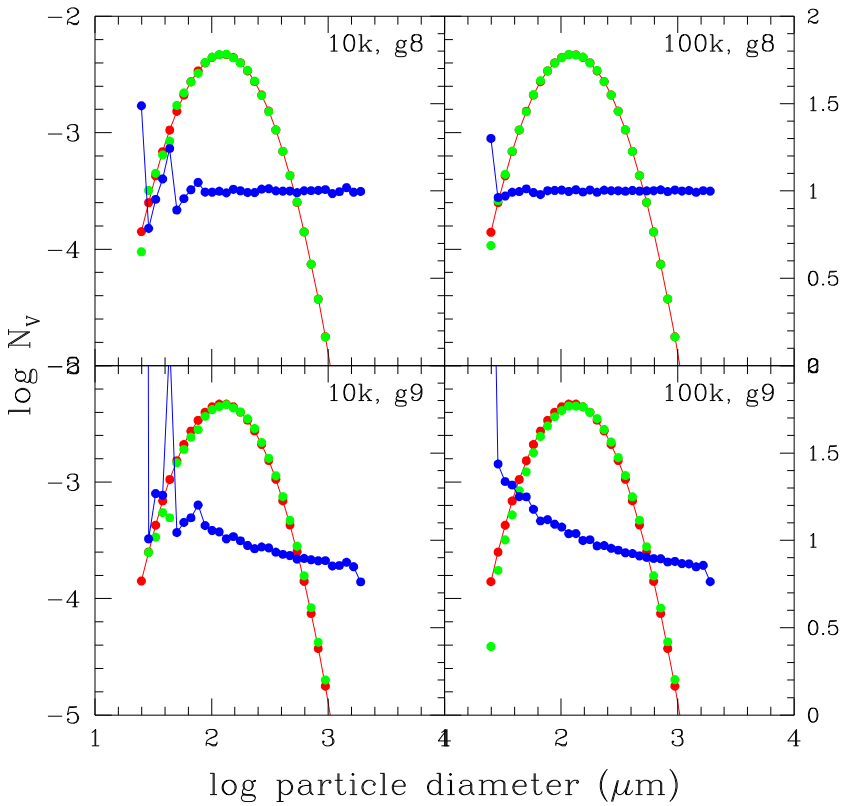

Fig. 8. This figure has the same structure as Fig. 7 but here we look at results from 10000 and 100000 randomly obtained "measurements," as indicated. (Color figure can be viewed at wileyonlinelibrary.com.)

(1983) includes yet another thin-section-related effect: "capping," in which caps cut very close to the "top" or "bottom" of a particle, where curvature is strong, have a bias to smaller effective diameters or even to being missed. This effect seems to provide mostly a fine-tuning parameter and we will not include it.

TESTING AND VALIDATION

We tested the various algorithms by comparison with a random-slicing technique. Both delta function N_V distributions, and lognormal distributions, were used as inputs. The delta functions represented one particle per diameter bin, sometimes in two or more different diameter bins, per (the same) unit volume. The lognormal distributions in diameter D had mean m and width w, defining the parameters $\mu = \log(m^2/\sqrt{m^2+w^2})$ and $\sigma = \sqrt{\log(1+w^2/m^2)}$:

$$N_V(D)/\Delta = \frac{C}{D\sigma\sqrt{2\pi}} \exp^{-(\log D-\mu)^2/2\sigma^2}. \quad (16)$$

Note the expression for N_V/Δ is a distribution per unit volume, per unit diameter, so must be multiplied by the bin width (which might vary, in the case of geometric binning) to create a binned N_V in the spirit of this approach. Then the number of apparent diameters per bin becomes (to within an arbitrary constant, depending on the number of cuts):

$$N_A(d_i) = \sum_n \sum_j N_V(D_j)(D_j - D_{j-1}) \times (D(j)/D_{\max})\delta(d_i - d_{i,n}) \quad (17)$$

where $d_{i,n} = D_j\sqrt{1-x_n^2}$ is the apparent diameter (lying in bin i) resulting from the nth cut through a single sphere of diameter D_j, x_n is a random number between 0 and 1, and the Kronecker delta δ represents binning of the nth cut into the appropriate apparent diameter bin i. As mentioned earlier, the term $(D(j)/D_{\max})$ accounts for the sampling bias (Eisenhour 1996): any given sphere of diameter $D(j)$ smaller than the maximum $D_{\max}$ is sampled less often by that factor. The bin width Δ is written as $(D_j - D_{j-1})$, to allow for geometric binning schemes where it is not constant. Figure 2 shows typical results for a delta function initial size distribution N_V. The shape of the apparent diameter distribution is characteristic of spheres (Weibel 1979, 1980), and the mode value depends on the bin width.

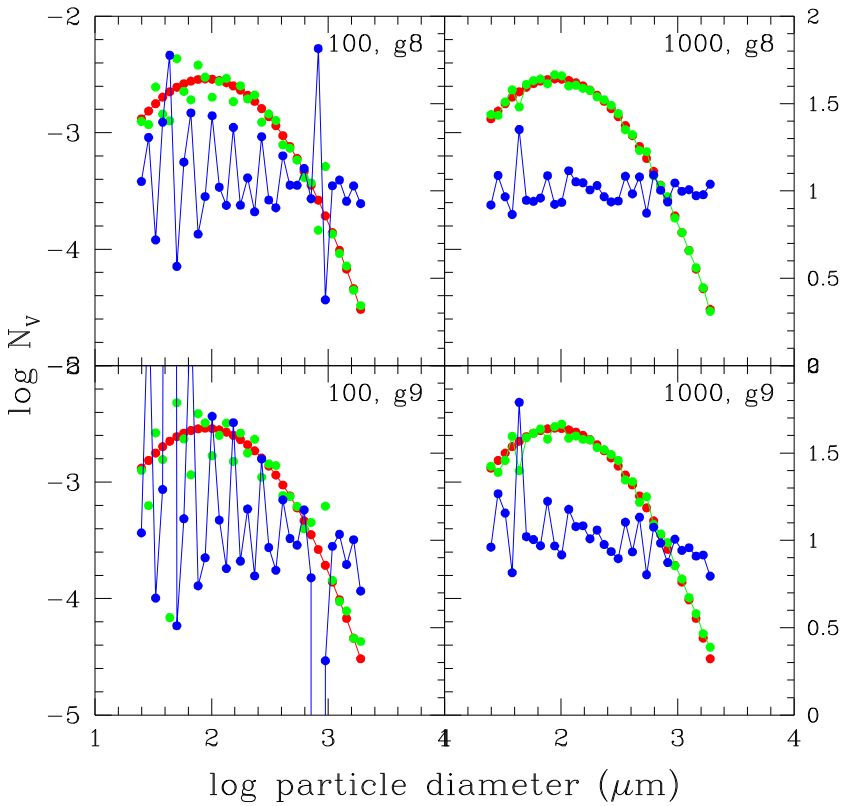

Fig. 9. This figure is similar to Fig. 7 but the initial N_{Vo} has a mean diameter of 150 μm and width of 200 μm. (Color figure can be viewed at wileyonlinelibrary.com.)

We first tested three different inversion techniques on a lognormal distribution (Equation 16) with parameters not too different from recent recovered Allende samples (Fisher et al. 2014). We "sectioned" the initial lognormal $N_{Vo}(D)$ (mean diameter of 160 and width of 160) numerically with large numbers ($N_S = 500000$) of random sections *per size bin* to get "ideal" apparent diameter distributions $N_A(D)$. Note in Fig. 3 that the apparent diameter distributions observed in sections (blue) are dominated by larger particles that characterize the actual sphere volume distributions (red and green), as discussed above. Of course, knowing this, observational counts can also be analyzed by comparison of forward models *of apparent diameter distributions* obtained using random sectioning techniques on different candidate true diameter distributions. This "forward approach" might be a promising approach to modeling core-rim-thickness relationships from 2D section data.

We then inverted the $N_A(d)$ distributions of Fig. 3 using three different algorithms discussed above (Equations 6, 8, and 9). In Fig. 3, all quantities are normalized by dividing by the respective total counts. For arithmetically binned profiles with $\Delta = 25$ (Fig. 3, left), the green (recovered N_V) curve almost completely overlaps the red (initial N_{Vo}) curve. In Fig. 3 (right) the original lognormal distribution N_{Vo} (in red) is binned geometrically. The randomly sectioned $N_A(d)$ (500000 sections per N_V bin) is shown in blue. We plot the recovered N_V as obtained using two techniques: the upper bin boundary method of Equation 8 (green solid) and the geometric midpoint method of Equations 9 (green dashed). The most obvious message of Fig. 3 is the overrepresentation of large particles in apparent diameter distributions with respect to the true distributions.

Next we compare the accuracy of the inversions using the three techniques, starting with the random-section generated N_A as described above, for three different lognormal N_{Vo}. In Figs. 4–6, the blue curve is now the ratio of the initial N_{Vo} distribution (red) to the recovered N_V (green). The geometric binning approach of Equation 8 does the most systematically unbiased job of reproducing the initial distribution for these cases. The geometric technique of Equations 9 significantly underestimates the smaller particles for narrower distributions (Fig. 4), and the arithmetic technique of Equations 6 overestimates the smallest particles for broad distributions (Fig. 6).

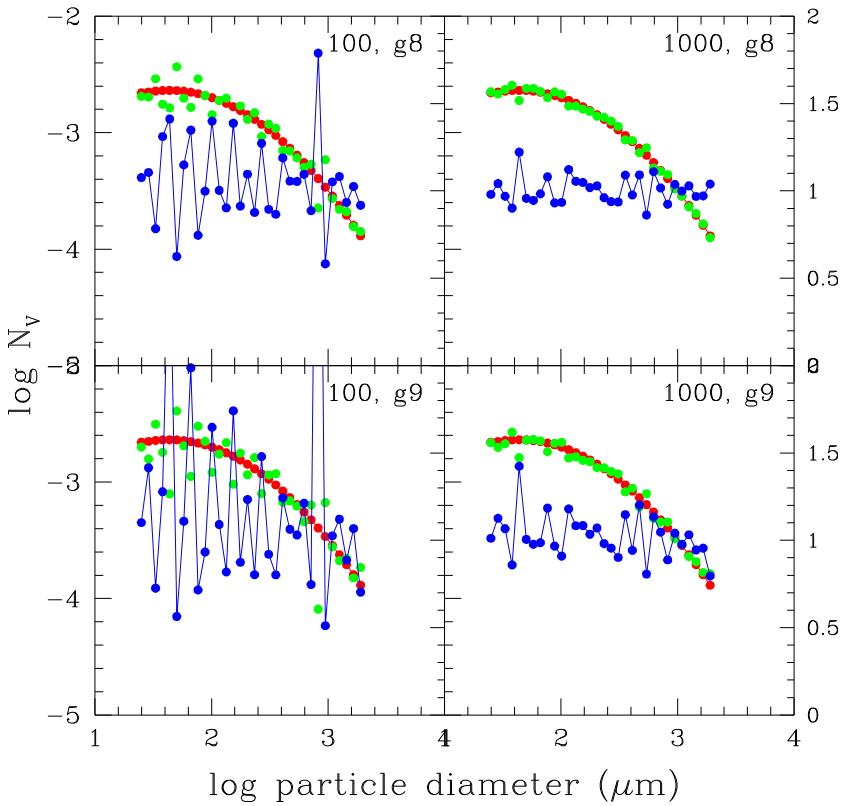

Fig. 10. This figure is similar to Fig. 7 but the initial N_{Vo} has a mean diameter of 150 μm and width of 500 μm. (Color figure can be viewed at wileyonlinelibrary.com.)

OBSERVATIONAL SAMPLING: REQUIREMENTS FOR ACCURACY

Here we give two different kinds of assessment of how many measurements of apparent diameter are needed to get reliable estimates of the underlying true diameter distribution. We use geometric binning with $c = 1.15$ and compare the inversions using Equation 8 with those done using Equations 9 (Figs. 7–10); arithmetic binning gives similar results (data not shown). The colors for the three curves are as before (red is the initial N_{Vo}, green is the recovered N_V, and blue is the ratio N_{Vo}/N_V). Here, the number densities and diameters are plotted on a log-log scale so that one can see the low-end behavior better, where the bin width is narrower.

For these figures, in the upper panels Equation 8 was used to recover N_V, and in the lower panels Equations 9 was used. The number of "measurements" N_S (expressed as random cuts *per* N_{Vo} *bin*) used to create the N_A distribution is given at the top of the columns. In Figs. 7, 9, and 10, the first column (N_S = 100 random sections per true diameter bin) is adequate to give a fair idea of the underlying size distribution and, as N_S increases, the recovered N_V becomes very well defined. In Figs. 7 and 8 where the lognormal width = 100 μm, we see that defining D_j at the upper end of the jth bin (Equation 8) gives better results as N_S increases than defining D_j by the geometric midpoint (Equations 9). The systematic downward trend in the N_{Vo}/N_V ratio resulting from Equations 9, seen in Figs. 4–6, is seen here as well. It is important to note that in Figs. 7–10 the initial and recovered distributions have 32 size bins, making for a nicely resolved result but containing a total number of measurements roughly 32 times the numbers labeling each plot. However, this test is slightly unrealistic, because in reality the less abundant sizes are sampled less often than the abundant sizes.

A Better Estimate of Observational Needs

To get an assessment that is closer to a real observation, we use a standard technique to model the observation as a number-limited random sampling of the underlying N_A distribution. This approach is more realistic because it provides more samples of the most common apparent diameters, as would be the case in reality, whereas the above approach contains as many samples of rare size bins as of bins containing common sizes. We first construct a "best case" $N_{Ao}(d)$ from 500k random cuts per size bin in N_{Vo}, and interpolate it onto

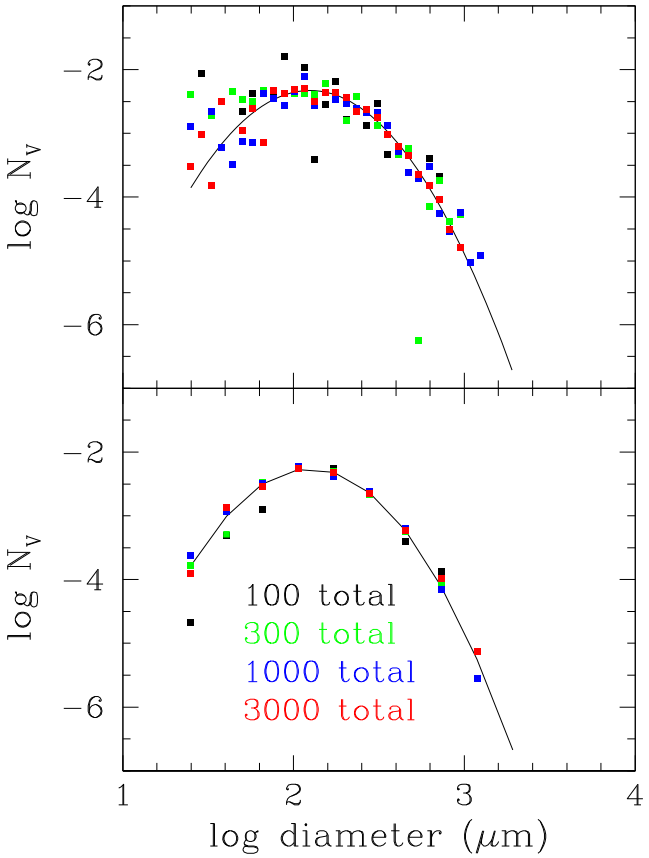

Fig. 11. To indicate the sample size needed to obtain reliable statistics, this figure plots inversions from four different simulated "measurement samples" of 100, 300, 1000, and 3000 chondrule apparent diameters, as binned into 32 bins (top) and 10 bins (bottom). The black curve represents the true initial diameters for a narrow lognormal distribution with mean diameter 150 μm and width 100 μm. See text for explanation of the sampling technique. (Color figure can be viewed at wileyonlinelibrary.com.)

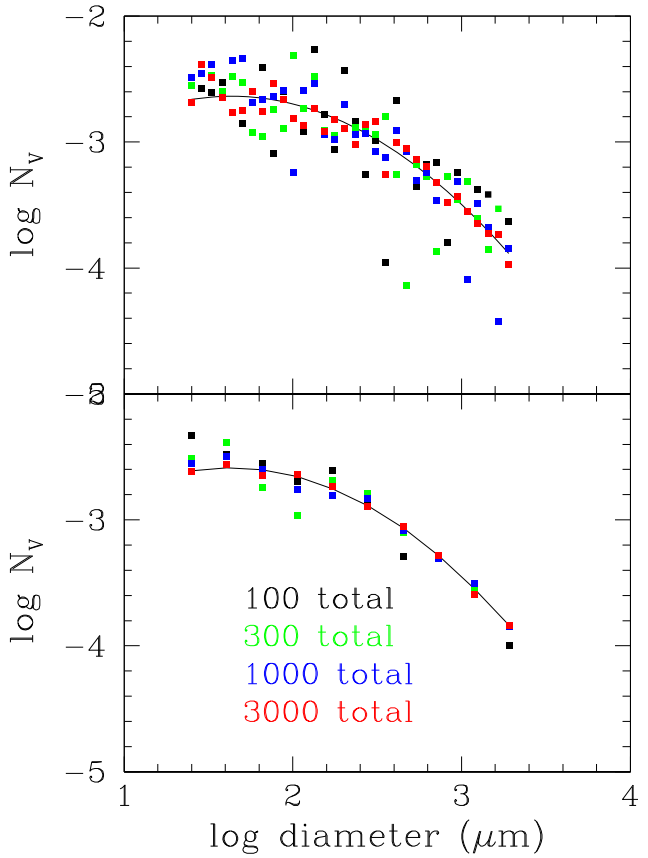

Fig. 12. To indicate the sample size needed to obtain reliable statistics, this figure plots inversions from four different simulated "measurement samples" of 100, 300, 1000, and 3000 chondrule apparent diameters, as binned into 32 bins (top) and 10 bins (bottom). The black curve represents the true initial diameters for a broad lognormal distribution with mean diameter 150 μm and width 500 μm. See text for explanation of the sampling technique. (Color figure can be viewed at wileyonlinelibrary.com.)

a uniform grid. We compute the normalized cumulative function

$$I(d) = \int_0^d N_{Ao}(x)\mathrm{d}x, \tag{18}$$

where $I(d_{\max}) = 1$. We then draw N_S random numbers uniformly distributed between 0 and 1; each of these represents a value of $I(d)$, which in turn corresponds to a specific value of d. The binned histogram of these "measurements" has the underlying probability distribution $N_{Ao}(d)$. We then use Equation 8 to recover N_V from these histograms and compare it with the initial distribution N_{Vo}. The results are shown in Figs. 11 and 12 for two different lognormal distributions, each showing three different values of N_S (here, N_S is the total number of apparent diameter measurements across the entire observed histogram). We show results for 10-bin histograms as well as the previous 32-bin histograms.

Overall these results suggest that 100 measurements of apparent diameter can capture a decent representation of a narrow, well-resolved particle size distribution, at least with 10 diameter bins, as far as obtaining a crude mean size and width. Broader, more subtle distributions require 300 measurements. Probably, 300 measurements or more is a practical and desirable goal for quantitative work dedicated to looking for variations from one chondrite to another and/or within different sectors of a given chondrite or matched samples. In the future, automated or crowd-sourced counting schemes tabulating thousands of objects would be needed to reveal subtle place-to-place variations or multiple modes or "bumps."

SUMMARY

This paper presents new algorithms for inverting histograms of particle apparent diameters in 2D sections into the actual underlying 3D volume size distributions they represent. Useful results can still be obtained working with 2D sections, as long as their biases are realized and they are compared with random slicing forward models of actual distributions. We find that one particular inversion using geometrical binning (Equation 8) provides the least biased overall results. We show that more than 100 measurements of the 2D apparent diameter distribution are required to obtain good results for the underlying true diameter distribution.

Acknowledgments—We are grateful to Quentin Williams for pointing out the work of Cruz-Orive; to Don Eisenhour, Michael Enfield and Wuwei Liang for helpful conversations; and to Seth Teitler for pointing out a notational error which rippled through the paper. Jon Friedrich and Derek Sears provided internal reviews that improved the paper; Justin Simon and Denton Ebel also provided useful feedback. We also thank Jon Friedrich for his very thorough journal review that included actually smoke-testing the fortran codes, as well as Michael Cato at JSC, who retested them based on newly written documentation and added useful comments to the documentation. We acknowledge the invaluable support of the Ames Research Center Research Library staff, in particular Dan Pappas and Kathy Ponce, for helping us locate and acquire diverse reference materials. This kind of expert information access and retrieval is essential to a person working out of their narrow discipline, even in an age when supposedly "everything is online." This work was supported by NASA's Origins of Solar Systems Program.

Editorial Handling—Dr. Josep Trigo-Rodríguez

REFERENCES

Cruz-Orive L.-M. 1976. Particle size-shape distributions: The general spheroid problem; I: Mathematical model. *Journal of Microscopy* 107:235–253.

Cruz-Orive L.-M. 1978. Particle size-shape distributions: The general spheroid problem. II. Stochastic model and practical guide. *Journal of Microscopy* 112:153–157.

Cruz-Orive L.-M. 1983. Distribution-free estimation of sphere size distributions from slabs showing overprojection and truncation, with a review of previous methods. *Journal of Microscopy* 131:265–290.

Dodd R. T. 1976. Accretion of the ordinary chondrites. *Earth and Planetary Science Letters* 30:281–291.

Eisenhour D. D. 1996. Determining chondrule size distributions from thin-section measurements. *Meteoritics & Planetary Science* 31:243–248.

Fisher K., Tait A., Simon J., and Cuzzi J. 2014. Contrasting size distributions of chondrules and inclusions in Allende CV3 (abstract #1777). 45th Lunar and Planetary Science Conference. The Woodlands, Texas.

Friedrich J. M., Weisberg M. K., Ebel D. S., Biltz A. E., Corbett B. M., Iotzov I. V., Khan W. S., and Wolman M. D. 2014. Invited review. *Chemie der Erde*, doi:10.1016/j.chemer.2014.08.003; see also eprint arXiv:1408.6581.

Goldsmith P. L. 1967. The calculation of true particle size distributions from the sizes observed in a thin slice. *British Journal of Applied Physics* 18:813–830.

Grossman J. N., Rubin A. E., Nagahara H., and King E. A. 1988. *Properties of chondrules. In Meteorites and the early solar system*, edited by Kerridge J. F. and Matthews M. S. Tucson, Arizona: University of Arizona Press. pp. 619–659.

Hezel D. C., Russell S. S., Ross, A. J., and Kearsley A. T. 2008. Modal abundances of CAIs: Implications for bulk chondrite element abundances and fractionations. *Meteoritics & Planetary Science* 43:1879–1894.

Hughes D. W. 1978a. Chondrule mass distribution and the Rosin and Weibull statistical functions. *Earth and Planetary Science Letters* 39:371–376.

Hughes D. W. 1978b. A disaggregation and thin section analysis of the size and mass distribution of the chondrules in the Bjurbole and Chainpur meteorites. *Earth and Planetary Science Letters* 38:391–400.

Kuebler K. E., McSween H. Y., Carlson W. D., Hirsch D. 1999. Sizes and masses of chondrules and metal-troilite grains in ordinary chondrites: Possible implications for nebular sorting. *Icarus* 141:96–106.

Liang W. and Enfield M. 2011. Estimating the probabilistic size and shape distributions of 3D anomalies from sectioning measurements using the stereological inverting approach, Paper #GT2011-46653, Proceedings of the ASME Turbo Expo 2011, June 6-10 2011, Vancouver.

Metzler K., Bischoff A., and Stoeffler D. 1992. Accretionary dust mantles in CM chondrites – Evidence for solar nebula processes. *Geochimica et Cosmochimica Acta* 56:2873–2897.

Nelson V. E. and Rubin A. E. 2002. Size-frequency distributions of chondrules and chondrule fragments in LL3 chondrites: Implications for parent-body fragmentation of chondrules. *Meteoritics & Planetary Science* 37:1361–1376.

Rubin A. E. 1989. Size-frequency distributions of chondrules in CO3 chondrites. *Meteoritics* 24:179–189.

Rubin A. E. and Grossman J. N. 1987. Size-frequency distributions of EH3 chondrules. *Meteoritics* 22:237–251.

Rubin A. E. and Keil K. 1984. Size-distributions of chondrule types in the Inman and Allan Hills A77011 L3 chondrites. *Meteoritics* 19:135–143.

Saltykov S. 1967. The determination of the size distribution of particles in an opaque material from a measurement of the size distribution of their thin sections. In *Stereology*, edited by Elias H. New York: Springer-Verlag. pp. 163–173.

Schneider D. M., Benoit P. H., Kracher A., and Sears D. W. G. 2003. Metal size distributions in EH and EL chondrites. *Geophysical Research Letters* 30:2-1–2-4.

Underwood E. E. 1970. *Quantitative stereology*. Massachusetts: Addison-Wesley. Addison Wesley: Boston, MA.

Weibel E. R. 1979. *Stereological methods, volume 1: Practical methods for biological morphometry*. Cambridge, Massachusetts: Academic Press.

Weibel E. R. 1980. *Stereological methods, volume 2: Theoretical foundations*. Cambridge, Massachusetts: Academic Press.

Wicksell S. D. 1925. The corpuscle problem, I: Case of spherical corpuscles. *Biometrica* 17:84–99.

SUPPORTING INFORMATION

Additional supporting information may be found in the online version of this article:

Data S1. Replication files.